Applied Catalysis B: Environmental 91 (2009) 610–618

Contents lists available at ScienceDirect

Applied Catalysis B: Environmental

journal homepage: www.elsevier.com/locate/apcatb

Support effect on the low-temperature hydrogenation of benzene over PtCo bimetallic and the corresponding monometallic catalysts

Shuliang Lu [a,c], William W. Lonergan [b], Yuexiang Zhu [a,*], Youchang Xie [a], Jingguang G. Chen [b,*]

[a] Beijing National Laboratory for Molecular Sciences, State Key Laboratory for Structural Chemistry of Unstable and Stable Species, College of Chemistry and Molecular Engineering, Peking University, Beijing 100871, China
[b] Department of Chemical Engineering, Center for Catalytic Science and Technology (CCST), University of Delaware, Newark, DE 19716, USA
[c] Institute of Theoretical and Computational Chemistry and Center for Computational Science and Engineering, Peking University, Beijing 100871, China

ARTICLE INFO

Article history:
Received 14 April 2009
Received in revised form 20 June 2009
Accepted 29 June 2009
Available online 8 July 2009

Keywords:
Benzene
Hydrogenation
Bimetallic
PtCo
EXAFS

ABSTRACT

PtCo bimetallic and Co, Pt monometallic catalysts supported on γ-Al_2O_3, SiO_2, TiO_2 and activated carbon (AC) were prepared and evaluated for the hydrogenation of benzene at relatively low temperatures (343 K) and atmospheric pressure. Results from flow reactor studies showed that supports strongly affected the catalytic properties of different bimetallic catalysts. AC supported PtCo bimetallic catalysts exhibited significantly better performance than the other bimetallic catalysts, and all the bimetallic catalysts possessed higher activity than the corresponding monometallic catalysts. Results from CO chemisorption and H_2-temperature-programmed reduction (H_2-TPR) studies suggested that different catalysts possessed different properties in chemisorption capacity and reduction behavior, and AC supported PtCo catalysts possessed significantly higher CO chemisorption capacity compared to the other catalysts. Extended X-ray absorption fine structure (EXAFS) and transmission electron microscopy (TEM) analysis provided additional information regarding the formation of Pt–Co bimetallic bonds and metallic particle size distribution in the PtCo bimetallic catalysts on different supports.

1. Introduction

Hydrogenation of aromatic hydrocarbons to saturated cyclic products is of significant importance both in environmental protection and in industrial processes. Currently, this reaction is of practical interest due to the increasing demand for suppression of the benzene content in petroleum fuels, especially in gasoline and diesel [1]. Because of the resonance stabilization of the monoaromatic ring, kinetic and thermodynamic results show that polyaromatics are more easily reduced than benzene under moderate conditions [1]. Thus, the hydrogenation of benzene is a useful model reaction for identifying promising catalysts for the hydrogenation of arenes. Furthermore, the cyclohexane product from benzene hydrogenation is one of the key intermediates in the synthesis of Nylon-6 and Nylon-66 [2]. Therefore, the development of active catalysts for the hydrogenation of benzene is of both fundamental and practical importance.

Catalysts based on group VIII metals, such as Ni [3–13], Fe [14–16], Pt [17,18], Pd [19,20], Ru [21–23] and Co [24–29], have been used for the hydrogenation of benzene. Among them, Ni- and Pt-based catalysts have been extensively studied and implemented in commercial processes. Although supported cobalt catalysts have been widely used in Fischer–Tropsch synthesis [30,31], relatively few studies have been reported regarding benzene hydrogenation over Co-based catalysts.

Supported cobalt catalysts have been investigated carefully in Fischer–Tropsch synthesis, including the effects of support variables, metal loading and noble metal promoters [32–38]. Jacobs et al. reported that significant support interactions on the reduction of cobalt oxide species followed the trend of $Al_2O_3 > TiO_2 > SiO_2$, and the addition of Pt to Co/Al_2O_3 catalysts increased the percentage reduction of cobalt and lowered the reduction temperature observed in H_2-TPR [34]. The effect of Pt–Co bimetallic formation has been studied carefully using EXAFS [35,38]. In these studies, no Pt–Pt coordination was found and Pt atoms mostly interact with Co forming Pt–Co bimetallic bonds. It was concluded that Pt is likely to be situated on the edge of the cluster, and the reduction occurs on Pt first, with subsequent spill-over of hydrogen atoms to the cobalt oxide species that leads to a decrease in reduction temperature.

In our previous work, PtCo, PtNi bimetallic and Co, Ni, Pt monometallic catalysts supported on γ-Al_2O_3 were compared and the results suggested that PtCo bimetallic catalysts possessed much higher activity, defined by dividing conversion by the

* Corresponding author.
E-mail addresses: zhuyx@pku.edu.cn (Y. Zhu), jgchen@udel.edu (J.G. Chen).

0926-3373/$ – see front matter © 2009 Published by Elsevier B.V.
doi:10.1016/j.apcatb.2009.06.036

amount of CO adsorbed per gram catalyst from CO chemisorption measurements for each catalyst, than PtNi bimetallic and Co, Ni, Pt monometallic catalysts for the hydrogenation of benzene at relatively low temperatures (343 K) [39]. In a more recent work [40], several silica supported Co-based bimetallic (PtCo, PdCo and RuCo) and the corresponding monometallic catalysts were evaluated for the low-temperature hydrogenation of benzene and the catalytic activities were correlated with the binding energies of benzene and atomic hydrogen on the metallic surfaces from density functional theory (DFT) calculations. Both the experimental and theoretical calculation results suggested that PtCo bimetallic catalyst possessed higher activity than other monometallic and bimetallic catalysts.

The observation of enhanced hydrogenation activity over PtCo is consistent with the fact that bimetallic catalysts often show properties that are distinctly different from those of the corresponding monometallic catalysts [41–45]. Many previous investigations combining fundamental surface science studies and theoretical calculations have been performed with the goal of correlating electronic properties of bimetallic surfaces with catalytic properties [43–54]. More recently, it has been demonstrated that Co/Pt(1 1 1) bimetallic surfaces [50,54], with Co atoms residing in the subsurface region in Pt(1 1 1), showed much higher activity for the hydrogenation of cyclohexene than the corresponding monometallic surfaces. The novel low-temperature hydrogenation pathway on the bimetallic surfaces has been correlated to the modification of the electronic properties due to the formation of the subsurface bimetallic structures [54].

The bridging of the materials gap between model surfaces and supported catalysts has always been a challenge, with one reason being that supported catalysts often exhibit different catalytic performance depending on the nature of the support materials. The main objective of the present work is to investigate the support effect on PtCo bimetallic and the corresponding monometallic catalysts for the low-temperature hydrogenation of benzene to expand our previous experimental and theoretical investigations on the PtCo bimetallic catalysts. Al_2O_3, SiO_2, TiO_2 and activated carbon (AC) supported PtCo bimetallic and Co and Pt monometallic catalysts were studied for the hydrogenation of benzene. Supports strongly affected the properties of Co-based catalysts for the hydrogenation of benzene. Results from the flow reactor studies showed that the activated carbon supported PtCo bimetallic catalysts exhibited much higher conversion than the others, and that all the bimetallic catalysts exhibited higher conversion than the corresponding monometallic catalysts on the same support. Furthermore, CO chemisorption, H_2-TPR, TEM and EXAFS were used to characterize the bimetallic catalysts and to determine the possible origin of the different hydrogenation activities of PtCo on the different supports.

2. Experimental

2.1. Catalyst preparation

All the catalysts were prepared by the impregnation method. The Al_2O_3 support was derived from the precursor of pseudo-boehmite calcined at 823 K for 5 h to achieve the γ-Al_2O_3 structure. TiO_2 was prepared by dropping aqueous solution of $Ti(SO_4)_2$ and 3 mol/L $NH_3{\cdot}H_2O$ simultaneously into a beaker containing a small amount of 0.5 mol/L NH_4HCO_3 solution with subsequent filtering and washing. The product was dried at 363 K and then calcined in a muffle furnace at 773 K for 4 h. The preparation method was described in detail in the previous literature [55]. The SiO_2 support was calcined at 973 K for 5 h. The activated carbon support was washed using 1 mol/L HNO_3 followed by deionized water before the impregnation process. The $Co(NO_3)_2{\cdot}6H_2O$ (A.R.) or $Pt(NH_3)_4(NO_3)_2$ (Acrös Organics, 99%) precursor was dissolved in deionized water and impregnated into the support (Al_2O_3, SiO_2, TiO_2 and activated carbon) to produce a catalyst of 10 wt.%Co or 1.2 wt.%Pt over different supports. The supported 1.2 wt.%Pt–10 wt.%Co bimetallic catalyst was prepared by co-impregnation using $Pt(NH_3)_4(NO_3)_2$ (Acrös Organics, 99%) and $Co(NO_3)_2{\cdot}6H_2O$ (A.R.) to produce a final catalyst with 1.2 wt.%Pt–10 wt.%Co over different supports. After the impregnation, the catalysts were dried at 383 K for 12 h, and then calcined in air for Al_2O_3, SiO_2 or TiO_2 supported catalysts and pretreated in N_2 for activated carbon supported catalysts at 773 K for 4 h.

2.2. Catalyst characterization

2.2.1. N_2 physisorption and CO chemisorption

The specific surface area, pore volume, and average pore diameter of the supports and supported catalysts were measured by BET methods using a Micromeritics ASAP2010C instrument. The N_2 physisorption isotherm and pore size distributions of the four catalyst supports are shown in Fig. 1 and the results are summarized in Table 1. The N_2 physisorption results of supported catalysts are listed in Table 2.

CO chemisorption experiments were also performed using the Micromeritics ASAP2010C instrument. A volumetric static method was used for CO chemisorption. Prior to CO chemisorption, the catalysts (~0.10 g, 60–80 mesh) were reduced in H_2 at 623 K (723 K for 10%Co/SiO_2, 10%Co/TiO_2 and 10%Co/Al_2O_3) for 1 h (6 h for 10%Co/SiO_2, 10%Co/TiO_2 and 10%Co/Al_2O_3) and then evacuated at 623 K for 3 h to desorb any hydrogen from the catalysts. After cooling to 308 K and holding for 1 h to stabilize the temperature, the CO adsorption isotherms were then measured to determine the CO uptake at 308 K in the pressure range of 50–450 Torr. An initial CO adsorption isotherm was achieved to measure the total amount of adsorbed CO (chemisorbed and physisorbed). The catalyst was then outgassed in the measurement unit and then a second CO adsorption isotherm was measured to evaluate the amount of physisorbed CO. The total chemisorbed amount of CO was deduced by subtracting the second isotherm from the first one and extrapolating the nearly horizontal difference curve to the uptake axis. The uptake of CO on the different supported catalysts is compared in Table 2. The calculation of metal dispersion was based on CO chemisorption and assumed stoichiometry of M:CO = 1:1 (M = Pt, Co). Because of the large amount of metal loadings and the uncertainty of stoichiometry in the catalysts, the dispersion values on these catalysts are not very meaningful and are listed in Table 2 to only provide a relative ranking of metal dispersion. However, the amount of adsorbed CO provides a quantitative comparison of the number of active sites among the various monometallic and bimetallic catalysts.

2.2.2. X-ray diffraction (XRD)

X-ray diffraction analysis was performed in a Rigaku D/MAX-200 X-ray powder diffractometer with Ni-filtered Cu Kα radiation at 40 kV and 100 mA. The crystallite sizes of Co_3O_4 oxides on different supports except activated carbon were calculated from line broadening with Scherrer equation.

2.2.3. Transmission electron microscopy (TEM)

TEM analysis was performed on spent catalysts using a JEOL 2010F equipped with a Schottky field emission gun operated at 200 keV, with an ultra-high resolution pole piece providing a point resolution of 1.9 Å. Imaging was performed in scanning mode (STEM) using a 20 nm camera length and a 0.5 nm diameter nanoprobe. Samples were prepared by grinding and suspending the catalysts in ethanol, and then a small amount of this solution

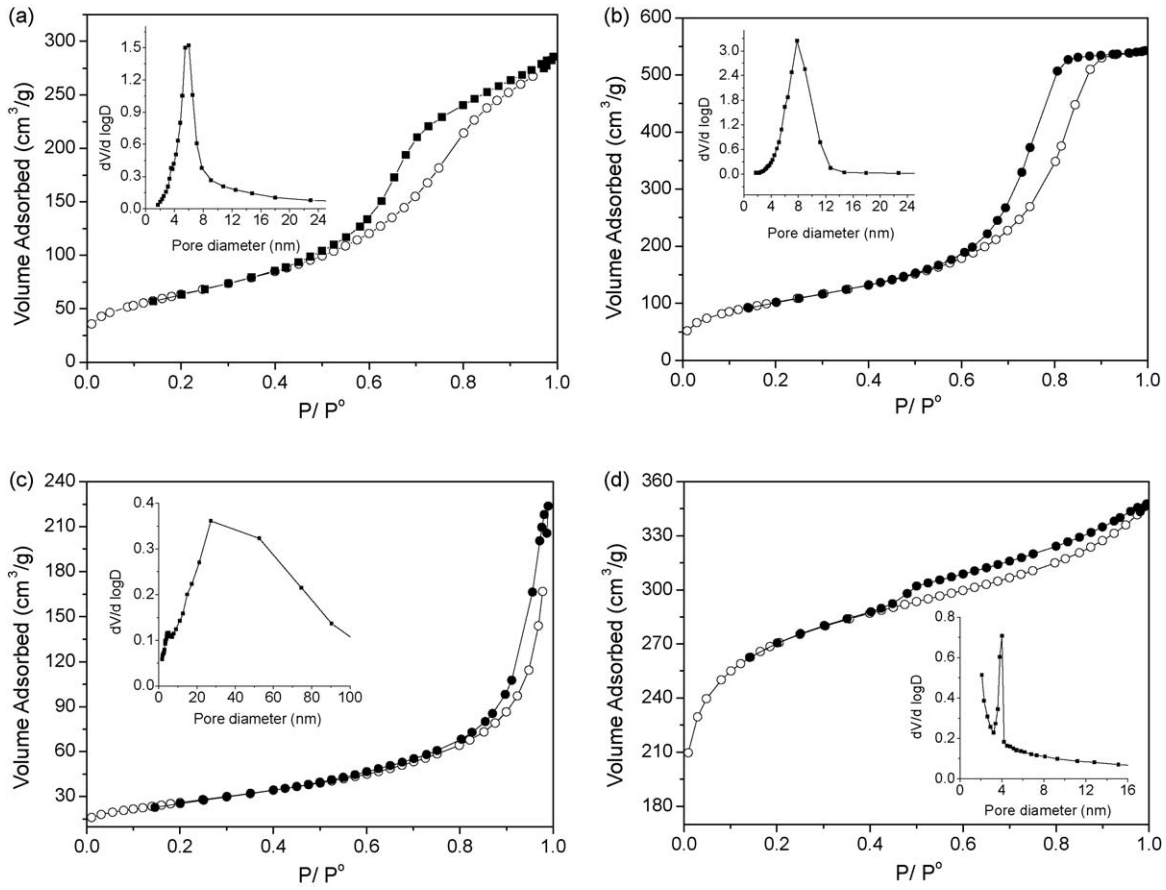

Fig. 1. Support nitrogen adsorption/desorption isotherms and pore size distributions calculated from the nitrogen desorption branches using the Barrett-Joyner-Halenda method: (a) Al_2O_3, (b) SiO_2, (c) TiO_2, and (d) activated carbon.

was dropped onto a carbon coated copper grid and allowed to dry before loading the sample in the TEM.

2.2.4. H_2-temperature-programmed reduction (H_2-TPR)

The TPR experiments were performed to determine the reduction behavior of the catalysts. The experiments were carried out in a U-shaped tubular quartz reactor heated by an electric furnace. 0.010 g of calcined catalyst (60–80 mesh) was exposed to a reducing gas consisting of 5.0 vol.% H_2 in Ar with a temperature ramp from 298 K to 1173 K at 10 K/min. The amount of hydrogen consumption was detected by a thermal conductivity detector (TCD). In order to calculate the degree of reduction, a reference sample (mechanical mixture of 20 wt.%CuO and 80 wt.%SiO_2) was also tested at the same time.

2.2.5. Extended X-ray absorption fine structure (EXAFS)

EXAFS measurements of the Pt L_{III}-edge were performed in order to confirm the presence of the Pt–Co bimetallic bonds. EXAFS experiments were performed on the X19A beamline at the National Synchrotron Light Source (NSLS), Brookhaven National Laboratory. Samples for EXAFS collection were prepared by pressing the powder catalysts into pellets using a force of approximately 3 t. Since TiO_2 and AC supported catalysts could not be pressed into self-supported pellets, Al_2O_3 was mixed with the catalyst before pressing to help hold the pellets together. In order to optimize the signal-to-noise ratio the pellet mass was calculated so that samples would have a thickness on the order of two absorption lengths. The samples were loaded into a reactor cell that allowed for *in situ* reduction as well as simultaneous collection of both transmission and fluorescence signals [56]. The catalysts were reduced under a diluted hydrogen flow (5% H_2 in He, 40 sccm) at 623 K for 1 h, and EXAFS data of the Pt L_{III}-edge were collected at room temperature. The incident and transmitted X-ray signals were collected with ionization chambers while the fluorescence signal was collected using a 12-channel germanium detector. The EXAFS spectra from the samples were calibrated to the Pt L_{III}-edge energy from a Pt reference foil collected in transmission mode.

A double crystal Si(1 1 1) monochromator was used to collect the EXAFS measurements. The EXAFS spectra were measured in three energy regions, each having a different step size and integration time: the pre-edge region from −150 to −25 eV before the edge (5 eV step size, 1 s integration time), the near-edge region from −25 eV before the edge to 40 eV past the edge (0.5 eV step size, 2 s integration time), and the post-edge region from 40 eV to 18 k (approximately 1450 eV) past the edge (0.05 k or ∼3 eV step size, 2 s integration time).

The fluorescence signal was analyzed using the IFEFFIT 1.2.11 data analysis package (Athena, Aretmis, Atoms, and FEFF6) [57,58]. The raw data was reduced in Athena by aligning each scan to the

Table 1
BET surface area, pore volume and average pore size of the catalyst supports.

Support	BET surface area (m^2/g)	Total pore volume (cm^3/g)	Micropore volume (cm^3/g)	Average pore diameter (nm)
Al_2O_3	228	0.44	0.00	7.7
SiO_2	370	0.84	0.00	9.1
TiO_2	94	0.35	0.00	14.7
AC	890	0.54	0.27	2.4

Table 2
Nitrogen physisorption and CO chemisorption results of the calcined catalysts.

Catalyst	Nitrogen physisorption			CO chemisorption	
	BET surface area (m^2/g)	Pore volume (cm^3/g)	Average pore diameter (nm)	CO uptake (μmol/g)	Dispersion[a] (%)
10%Co/Al_2O_3	193	0.33	6.9	15.3[b]	–
10%Co/SiO_2	314	0.58	7.4	16.8[b]	–
10%Co/TiO_2	69	0.25	14.8	1.9[b]	–
10%Co/AC	782	0.49	2.5	96.7	–
1.2%Pt–10%Co/Al_2O_3	193	0.33	6.8	41.7	2.93
1.2%Pt–10%Co/SiO_2	310	0.68	8.8	42.5	2.76
1.2%Pt–10%Co/TiO_2	70	0.32	18.2	33.8	2.09
1.2%Pt–10%Co/AC	739	0.44	2.4	395	23.3
1.2%Pt/Al_2O_3	227	0.39	6.9	24.5	39.8
1.2%Pt/SiO_2	360	0.73	8.1	13.3	21.6
1.2%Pt/TiO_2	87	0.28	12.8	26.2	42.5
1.2%Pt/AC	888	0.54	2.4	9.9	16.1

[a] Corrected by the degree of reduction, which was derived by H_2-TPR for PtCo bimetallic catalysts on Al_2O_3, SiO_2 and TiO_2. The dispersion of PtCo/AC was based on the assumption of 100% degree of reduction.
[b] Reduction time: 6 h.

reference foil, deglitching as necessary and averaging scans together to minimize experimental error. Background subtraction was also performed in Athena using the AUTOBK algorithm. Local structural information was obtained by Fourier-transforming the EXAFS signal into R-space and using Artemis to fit each data set to the theoretical standards generated in FEFF6 [59]. Both the Pt–Pt and Pt–Co contributions to the theoretical EXAFS were taken into account in constructing the model. The theoretical Pt–Pt photoelectron amplitudes and phases were calculated for the bulk Pt fcc structure. The Pt–Co contribution was modeled by replacing Pt with Co in the first nearest-neighbor shell. The seven parameters used in the fitting procedure were the correction to the edge energy, the coordination numbers of the Pt–Pt and Pt–Co bonds, corrections to their model interatomic distances and their mean-square deviations in interatomic distances (EXAFS Debye-Waller factors). The passive electron reduction factor $S_0^2 = 0.85$ which was fixed throughout the fitting of the PtCo catalysts, was determined by fitting the Pt reference foil.

2.3. Catalytic activity tests using flow reactor

The hydrogenation of benzene was carried out in a quartz glass reactor under atmospheric pressure at 343 K. The flow of benzene, controlled by a micro-syringe pump with a flow rate of 5.6 mmol/h, was carried by H_2 with a gas flow rate of 10 ml/min and N_2 with a gas flow rate of 40 ml/min. For each experiment, 50 mg of bimetallic or 100 mg of monometallic catalyst (60–80 mesh) was loaded into the flow reactor. Before the reaction, the catalyst was reduced under hydrogen (20 ml/min) and nitrogen (20 ml/min) mixture at 623 K (723 K for 10%Co/SiO_2, 10%Co/TiO_2 and 10%Co/Al_2O_3) for 1 h (6 h for 10%Co/SiO_2, 10%Co/TiO_2 and 10%Co/Al_2O_3). The product streams were analyzed by online gas chromatography equipped with a flame ionization detector (FID).

3. Results

3.1. XRD measurements

Fig. 2 shows the powder X-ray diffraction patterns of the calcined PtCo bimetallic catalysts on different supports. The peaks central at 36.8° and 44.2° were ascribed to Co_3O_4 and metallic Co, respectively. Based on the relative intensities of these two features, the Co elements appear to be mainly in the form of Co_3O_4 on Al_2O_3, SiO_2 and TiO_2, while in the form of metallic Co on activated carbon, which was attributed to the reduction of Co oxides by the carbon support in the preparation process of calcination at 773 K. The crystallite sizes of Co_3O_4 oxides on different supports except activated carbon were calculated from line broadening with the Scherrer equation [60]. From the calculation from XRD peaks at 36.8° the metal oxide size was estimated to be 13, 14 and 20 nm for Al_2O_3, SiO_2 and TiO_2 supported catalysts, respectively.

3.2. TEM measurements

TEM was used to characterize the particle size of the reduced bimetallic catalysts. To maximize the contrast between the metal nanoparticles and the support, high-angle annular dark field (HAADF) imaging was used to image the catalysts. Representative images of the PtCo bimetallic catalysts on different supports are shown in Fig. 3. Images of the four supported PtCo bimetallic catalysts all showed that the metallic particle size possessed wide distribution. The observed metallic particle sizes were predominately smaller than 10 nm. The average particle size of PtCo on TiO_2 appeared to be larger than that on other supports. Although there were some larger particles on PtCo/AC, many more small metallic particles could be found, which may account for the significantly higher CO chemisorption capacity.

3.3. H_2-TPR analysis

The reducibility of the calcined PtCo bimetallic and Co monometallic catalysts was studied by TPR and the reduction profiles are shown in Fig. 4. For the pure cobalt oxide (Co_3O_4), there

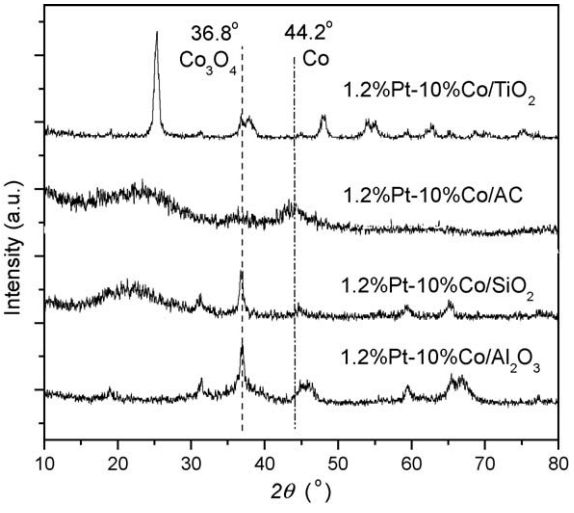

Fig. 2. XRD profiles of the calcined PtCo bimetallic catalysts on different supports.

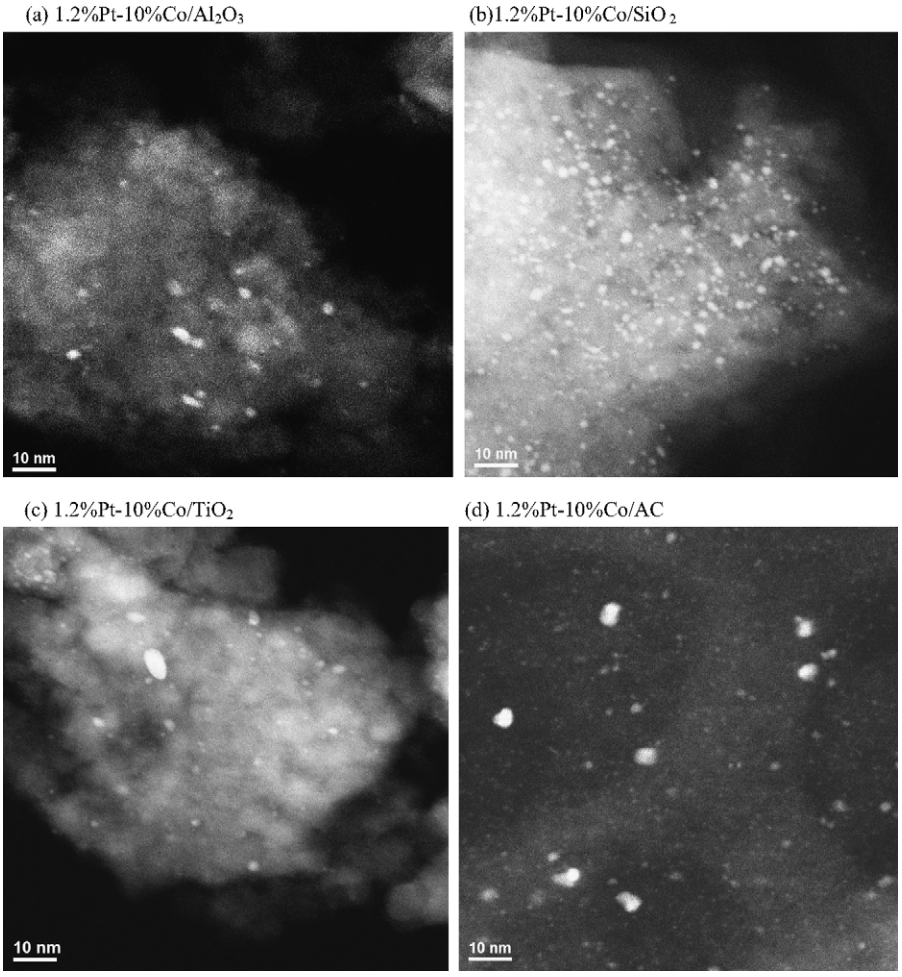

Fig. 3. TEM images of the reduced bimetallic catalysts: (a) 1.2%Pt–10%Co/Al_2O_3, (b) 1.2%Pt–10%Co/SiO_2, (c) 1.2%Pt–10%Co/TiO_2, and (d) 1.2%Pt–10%Co/AC.

were two major peaks around 700 K ascribed to the successive reduction of bulk Co_3O_4 to CoO to Co in the H_2-TPR profile [61]. Supported cobalt catalysts always show a much broader reduction temperature range because of the strong interaction between Co and the catalyst support [30,31]. For instance, the reduction process of alumina supported cobalt catalyst has been related to the following steps: Co_3O_4 clusters to CoO, bulk-like CoO to Co, and Co_xO_y–Al_2O_3 to Co metal [30]. Because AC supported catalysts were partially reduced in the preparation process, the hydrogen consumption could not be used to present the reduction behavior as that on the oxide supports. As shown in Fig. 4, monometallic Co catalysts had quite different reduction behavior on different supports. The 10%Co/TiO_2 and 10%Co/Al_2O_3 catalysts showed much broader reduction temperature range than 10%Co/SiO_2. For the PtCo bimetallic catalysts, the reduction temperature range became narrower and nearly the same for the three oxides supports, but SiO_2 supported catalysts possessed the lower onset of the reduction temperature range. For example, the reduction temperature of the first step decreased from approximately 620 K for the monometallic 10%Co/SiO_2 to 393 K for the 1.2%Pt–10%Co/SiO_2 bimetallic catalyst. The calculated degree of reduction of PtCo on Al_2O_3, SiO_2 and TiO_2 was 84%, 91% and 95%, respectively, which was used to calculate the corrected metal dispersion.

3.4. EXAFS analysis

EXAFS measurements were performed for the four 1.2%Pt–10%Co bimetallic catalysts in order to prove the presence of bimetallic bonds and to characterize the extent of bimetallic formation. The *k*-ranges used in the fitting were chosen in order to exclude regions of noise at high-*k*. The following *k*-ranges were used for the catalysts on the four supports: 2–15 (Al_2O_3), 3–14 (SiO_2), 2.5–10 (TiO_2), and 2.6–10 (AC). Spectra were k^2 weighted in order to obtain the best fits. A Hanning window with sill width of 2 $Å^{-1}$ was used in Fourier-transforming the spectra into R-space. The resulting transformations and Artemis fits to the data are presented in Fig. 5. Table 3 summarizes the results from the Artemis fitting.

In the bulk phase Co and Pt have first nearest neighbor distances of 2.506 Å (Co–Co) and 2.774 Å (Pt–Pt). Similar or slightly smaller values for the first nearest neighbor distances are expected in monometallic nanoparticles. In the case of bimetallic nanoparticles the first nearest neighbor distance should be a value in between the values for the two monometallic distances. The fitting results shown in Table 3 show Pt–Co distances between 2.54 and 2.56 Å for the different supported catalysts.

The Pt–Co coordination numbers were found to be 6.0 ± 0.7 on Al_2O_3, 5.3 ± 0.5 on SiO_2, 2.5 ± 0.6 on TiO_2, and 4.9 ± 1.2 on activated carbon, respectively. The ratio of Pt–Co to Pt–Pt coordination numbers characterizes the extent of bimetallic bond formation. For the Al_2O_3 and SiO_2 supported PtCo bimetallic catalysts this ratio of coordination numbers is greater than one, signifying that most Pt atoms are primarily coordinated with Co atoms. In comparison, the ratios for the TiO_2 and AC supported catalysts are less than one, suggesting that the first coordination shell around each Pt atom is mostly filled with other Pt atoms on these two supports.

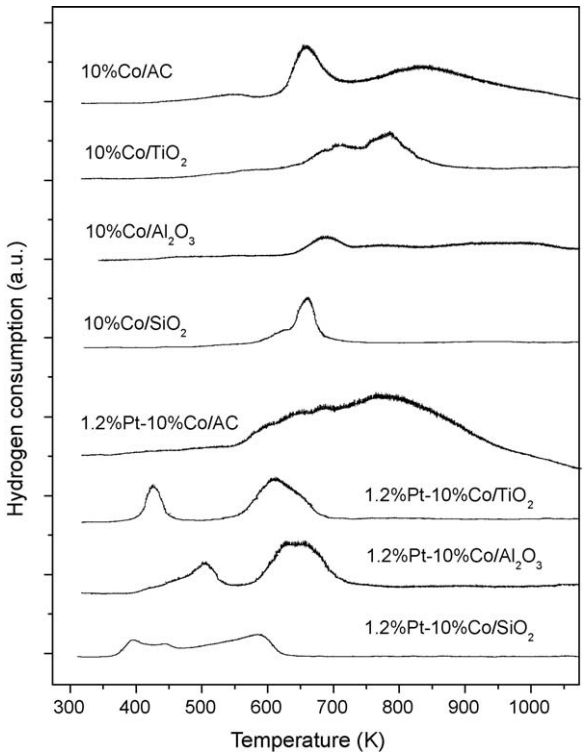

Fig. 4. H_2-TPR profiles of the calcined PtCo bimetallic and Co monometallic catalysts on different supports.

Table 3
Parameters derived from the EXAFS analysis of the bimetallic catalysts on different supports.

	$PtCo/Al_2O_3$	$PtCo/SiO_2$	$PtCo/TiO_2$	PtCo/AC
N(Pt–Pt)	0.6 ± 1.2	1.4 ± 0.8	5.7 ± 3.0	5.7 ± 0.8
N(Pt–Co)	6.0 ± 0.7	5.3 ± 0.5	2.5 ± 0.6	4.9 ± 1.2
R(Pt–Pt) Å	2.70 ± 0.03	2.70 ± 0.008	2.71 ± 0.07	2.67 ± 0.007
R(Pt–Co) Å	2.55 ± 0.04	2.56 ± 0.004	2.56 ± 0.01	2.54 ± 0.01
σ^2(Pt–Pt) Å^2	0.004 ± 0.006	0.003 ± 0.002	0.018 ± 0.008	0.011 ± 0.001
σ^2(Pt–Co) Å^2	0.005 ± 0.001	0.005 ± 0.001	0.008 ± 0.002	0.024 ± 0.003

3.5. Catalytic evaluation from flow reactor studies

The bimetallic and the corresponding monometallic catalysts were evaluated for benzene hydrogenation at 343 K and atmospheric pressure, which were rather moderate reaction conditions for benzene hydrogenation. 100 mg of monometallic catalysts and 50 mg of bimetallic catalysts were used for the hydrogenation tests. Cyclohexane was the only reaction product detected by online gas chromatography. As shown in Fig. 6b, the conversion of benzene was nearly zero for $10\%Co/Al_2O_3$ and $10\%Co/TiO_2$, about 2% for $10\%Co/SiO_2$ and 10%Co/AC, about 6% for $1.2\%Pt/SiO_2$ and $1.2\%Pt/Al_2O_3$, and nearly zero for $1.2\%Pt/TiO_2$ and 1.2%Pt/AC. In comparison, the supported PtCo bimetallic catalysts showed much higher conversion. Furthermore, the four supported PtCo bimetallic catalysts exhibited quite different catalytic activities. As shown in Fig. 6a, the conversion of benzene was about 60% for 1.2%Pt–10%Co/AC catalysts, which was much higher than Al_2O_3, SiO_2 or TiO_2 supported PtCo bimetallic catalysts. In summary, activated carbon supported PtCo bimetallic catalysts exhibited

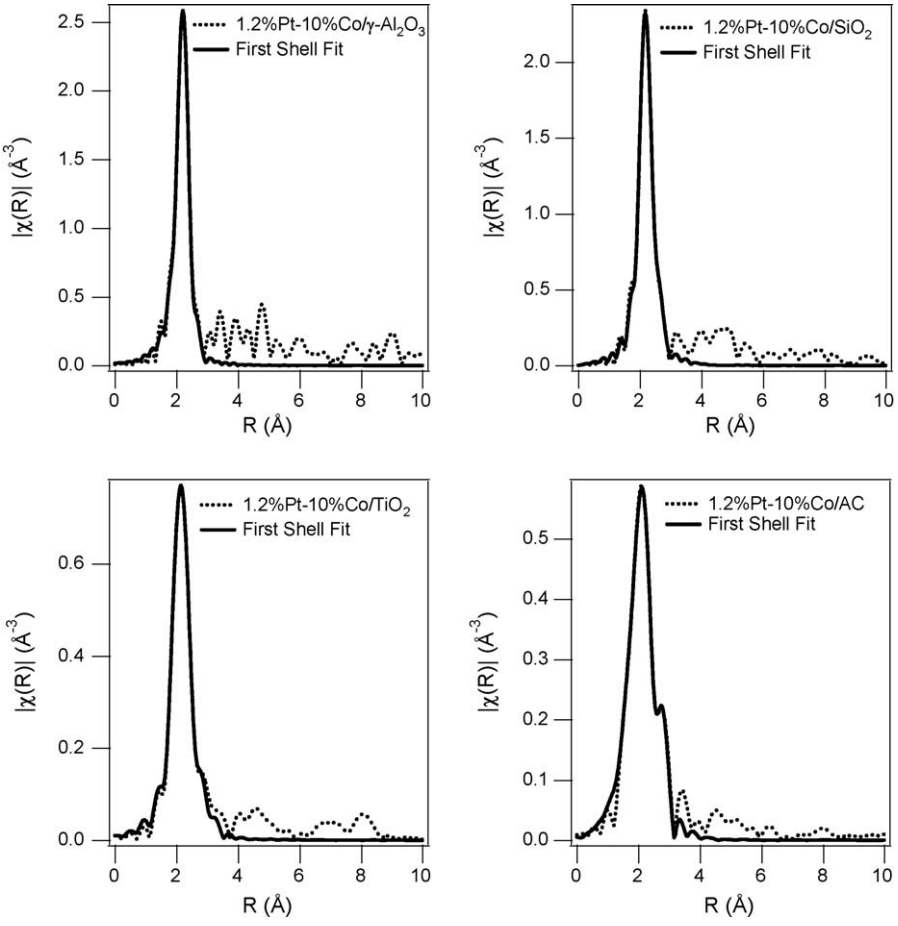

Fig. 5. Fourier-transformed k^2-weighted EXAFS function ($\chi(k)$) PtL_{III}-edge of 1.2%Pt–10%Co on γ-Al_2O_3, SiO_2, TiO_2, and AC.

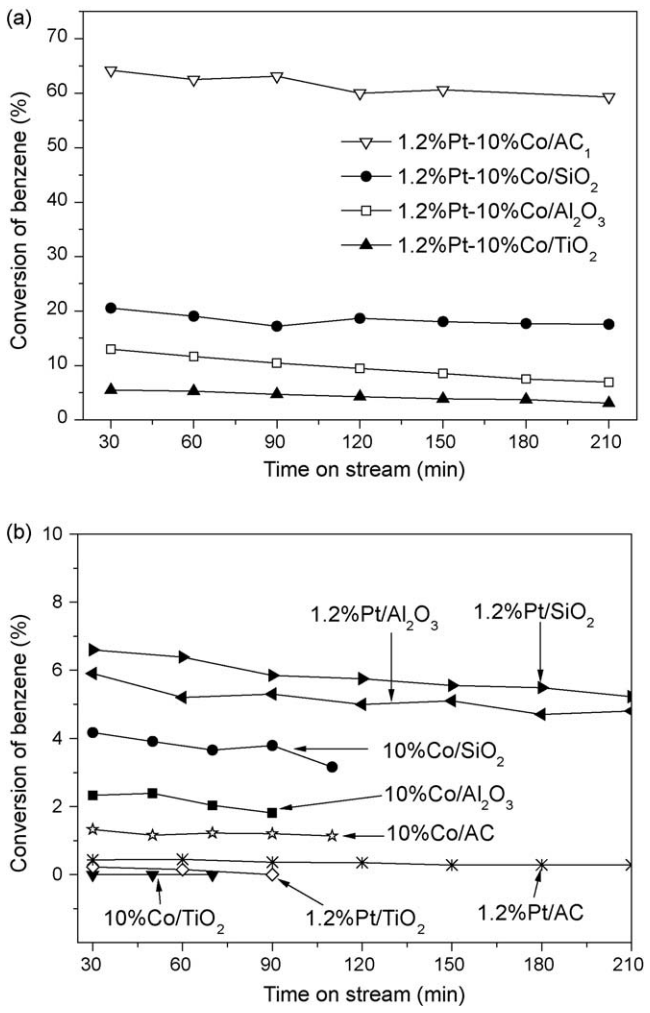

Fig. 6. Flow reactor study of benzene hydrogenation at 343 K: benzene conversion for (a) PtCo bimetallic and (b) Co or Pt monometallic catalysts on different supports. Experiment conditions: H_2:benzene = 5:1, catalyst amount: 50 mg for PtCo and 100 mg for Co or Pt.

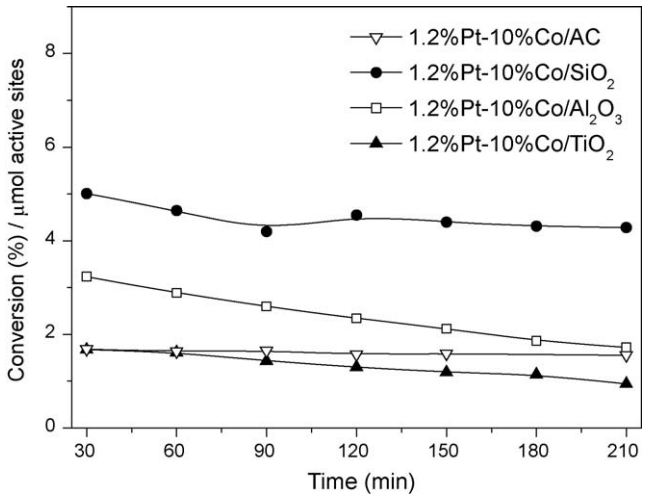

Fig. 7. Flow reactor study of benzene hydrogenation at 343 K: benzene conversion divided by the amount of CO adsorbed on the used catalysts calculated from CO chemisorption data.

Table 4
Comparison of benzene conversion, normalized conversion and activation barrier for PtCo bimetallic catalysts on different supports.

Catalyst	Conversion[a] (%)	Normalized conversion[b] (%/μmol active sites)	Ea (kJ/mol)
1.2%Pt–10%Co/Al_2O_3	10	2.6	33.7
1.2%Pt–10%Co/SiO_2	17	4.2	21.2
1.2%Pt–10%Co/TiO_2	4.7	1.4	43.1
1.2%Pt–10%Co/AC	63	1.7	40.9

[a] Conversion of benzene at 90 min on streams at 343 K in the flow reactor study.
[b] Conversion divided by amount of CO adsorbed from CO chemisorption measurements.

much better performance and the conversion of benzene over PtCo bimetallic catalysts followed the trend: AC > > SiO_2 > Al_2O_3 > TiO_2. Additionally, all the PtCo bimetallic catalysts showed much higher activities than the Co and Pt monometallic catalysts.

In order to correlate the conversion with the number of active sites on the catalyst surface for different supported PtCo bimetallic catalysts, the conversion of benzene was divided by the amount of CO adsorbed on the catalysts from CO chemisorption results to present the normalized catalytic hydrogenation activities. As shown in Fig. 7, the normalized activities followed the trend: SiO_2 > Al_2O_3 > TiO_2 ~ AC. The conversion and normalized conversion of benzene for the four bimetallic catalysts are listed in Table 4.

The apparent activation barriers for benzene hydrogenation reactions were estimated over different supported PtCo bimetallic catalysts, as shown in Fig. 8 and are listed in Table 4. The activation barrier for PtCo bimetallic on different supports showed the trend: SiO_2 < Al_2O_3 < TiO_2 ~ AC, which was consistent with the normalized catalytic hydrogenation activities shown in Fig. 7 and Table 4.

4. Discussion

Results presented above clearly demonstrate that catalyst supports strongly affect the properties of the PtCo bimetallic and the corresponding monometallic catalysts. The observation of SiO_2, Al_2O_3 and TiO_2 resulting in different support effects is consistent with literature reports. For example, Oyama coworkers have observed different effects by supporting manganese oxides on these three oxides [62].

As shown in Fig. 6, on a given support the bimetallic catalyst exhibits higher hydrogenation activity than the corresponding monometallic catalysts. The enhanced activity in PtCo could be attributed to the increased reducibility of Co oxides by the addition of Pt, and more importantly, to the formation of the Pt–Co bimetallic bonds. The PtCo bimetallic catalysts can be reduced much more easily than the monometallic Co catalysts, as demonstrated by the H_2-TPR results in Fig. 4. Consequently, the number of active sites is higher on the bimetallic catalysts, as indicated by the CO chemisorption results in Table 2. For example, the CO uptake value for the 1.2%Pt–10%Co/AC bimetallic catalyst is 395 μmol/g catalyst, which is much higher than the sum of uptake from the two monometallic catalysts, 96.7 and 9.9 μmol/g catalyst for 10%Co/AC and 1.2%Pt/AC, respectively. Similar increases in CO uptake are also observed for the other supported PtCo bimetallic catalysts listed in Table 2. The number of active sites from CO chemisorption capacity on the bimetallic catalysts follows the trend: AC > > SiO_2 ~ Al_2O_3 > TiO_2. Assuming that the CO chemisorption capacity is directly related to the hydrogenation activity, similar trend should be observed for the hydrogenation of benzene, as confirmed in Fig. 6a.

The enhanced hydrogenation activity in PtCo bimetallic catalysts is also consistent with previous surface science studies [49,50] and density functional theory (DFT) modeling [47,54] of low-temperature hydrogenation of cyclohexene on Co/Pt(1 1 1)

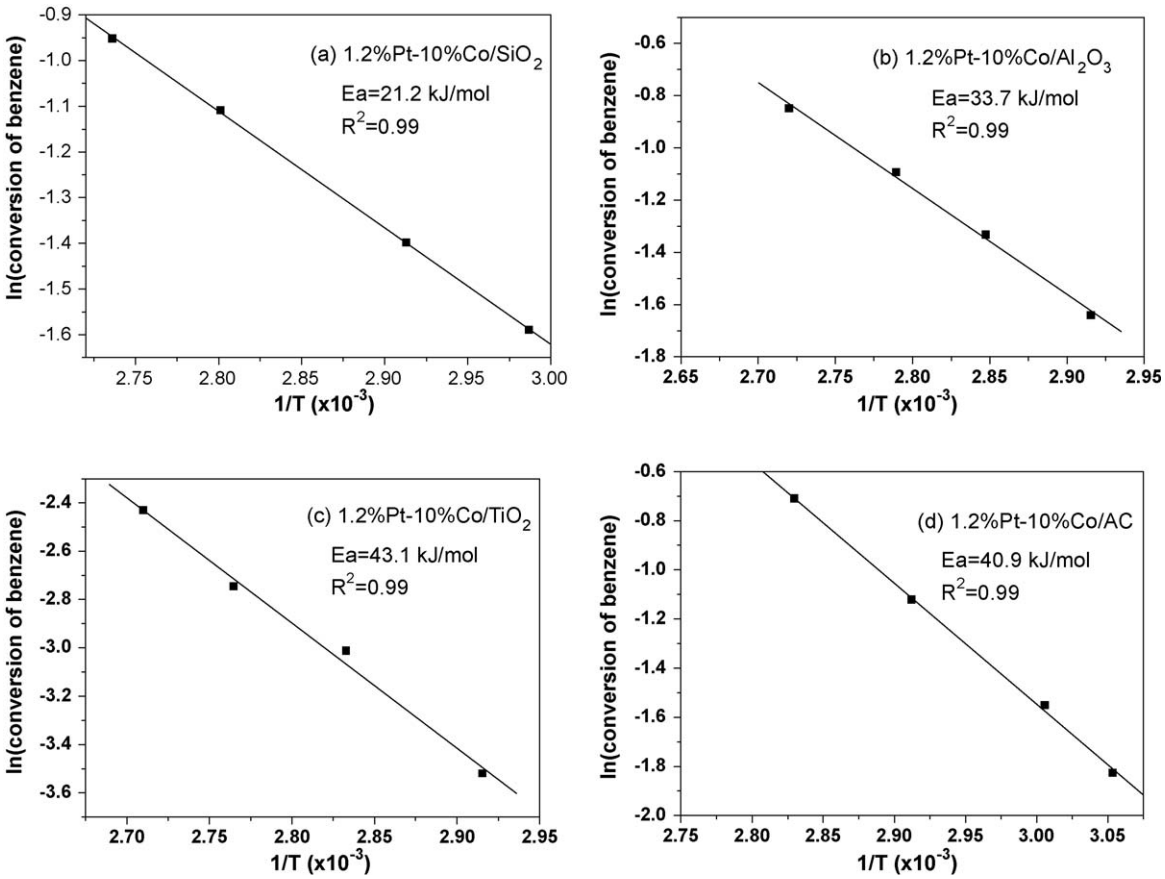

Fig. 8. Estimation of the apparent activation energy for benzene hydrogenation from flow reactor studies: (a) 1.2%Pt–10%Co/SiO_2, (b) 1.2%Pt–10%Co/Al_2O_3, (c) 1.2%Pt–10%Co/TiO_2, and (d) 1.2%Pt–10%Co/AC.

bimetallic surfaces. In these studies bimetallic surfaces, with a monolayer of Co residing directly underneath surface Pt atoms, have shown hydrogenation activity that is significantly higher than that of the parent metal, Pt or Co surfaces. The higher hydrogenation activity has been attributed to the relatively weak binding energies on the bimetallic surfaces for both atomic hydrogen and unsaturated hydrocarbons, such as cyclohexene and benzene, leading to a facile hydrogenation of the C=C bonds [40,47,54].

The extent of bimetallic formation appears to be different on the different supports. As shown in the EXAFS results in Table 3, on Al_2O_3 and SiO_2 most of the Pt atoms in the bimetallic catalysts are surrounded by Co atoms to form the Pt–Co bimetallic bonds, but there are less Pt–Co bonds for the PtCo/TiO_2 catalyst. These results are consistent with the flow reactor result that PtCo/TiO_2 shows the lowest activity among the three oxide-supported PtCo catalysts, as compared in Table 4.

The correlation between the Pt–Co coordination number (CN) and the hydrogenation activity is less clear on the AC support, which is characterized by relatively high CN values for both the Pt–Co and Pt–Pt bonds. The detection of the Pt–Co CN value of 4.9 in the EXAFS measurements qualitatively confirms the formation of the Pt–Co bond on AC. However, due to the presence of both small and large metallic particles in the TEM measurements, it is difficult to directly correlate the extent of Pt–Co bond formation from the EXAFS analysis. The presence of the smaller particles in PtCo/AC most likely provides more active sites for the chemisorption of CO and for the hydrogenation of benzene, leading to a higher benzene conversion than that of PtCo on the three oxide supports. On the other hand, the normalized conversion, based on the number of active sites for CO chemisorption, of PtCo/AC is lower than PtCo/Al_2O_3 and PtCo/SiO_2. This trend of normalized activities is consistent with the estimation of the apparent activation energy, where the values follow the trend: $SiO_2 < Al_2O_3 < TiO_2 \sim AC$. The synthesis and evaluation of more uniform PtCo particles on AC are needed to further understand the different support effects between AC and the oxide supports.

5. Conclusions

Al_2O_3, SiO_2, TiO_2 and activated carbon supported PtCo bimetallic and Co and Pt monometallic catalysts have been prepared by impregnation method and evaluated using a flow reactor for benzene hydrogenation at low temperatures and atmospheric pressure. Overall, catalyst supports strongly affect the catalytic activities of both monometallic and bimetallic catalysts. The results show that activated carbon supported PtCo bimetallic catalysts exhibit the best performance among all as-prepared bimetallic and monometallic catalysts, which is mostly attributed to the Pt–Co bimetallic formation and the very high CO chemisorption capacity. Furthermore, for all the supports, PtCo bimetallic catalysts show higher hydrogenation activities than the corresponding monometallic catalysts, supporting the argument from previous surface science and theoretical predictions that the formation of Pt–Co bimetallic bonds would result in higher hydrogenation activity than that of either Pt or Co.

Acknowledgements

The work was supported by the National Science Foundation of China (20440420577) and the Major State Basic Research

Development Program (Grant No. G2006CB806100). The authors from the University of Delaware acknowledge support from the U.S. Department of Energy (DE-FG02-00ER15104). Use of the National Synchrotron Light Source, Brookhaven National Laboratory, for the EXAFS experiments was supported by the U.S. Department of Energy (DOE/BES Grant No. DE-FG02-05ER15688).

Appendix A. Supplementary data

Supplementary data associated with this article can be found, in the online version, at doi:10.1016/j.apcatb.2009.06.036.

References

[1] A. Stanislaus, B.H. Cooper, Catal. Rev. Sci. Eng. 36 (1994) 75.
[2] J.-F. Le Page, Applied Heterogeneous Catalysis: Design, Manufacture, Use of Solid Catalysts, Technip, Paris, 1987, p. 291.
[3] R.Z.C. van Meerten, J.W.E. Coenen, J. Catal. 37 (1975) 37.
[4] R.Z.C. van Meerten, A.C.M. Verhaak, J.W.E. Coenen, J. Catal. 44 (1976) 217.
[5] H.A. Franco, M.J. Phillips, J. Catal. 63 (1980) 346.
[6] A. Jasik, R. Wojcieszak, S. Monteverdi, M. Ziolek, M.M. Bettahar, J. Mol. Catal. A Chem. 242 (2005) 81.
[7] A. Louloudi, J. Michalopoulos, N.H. Gangas, N. Papayannakos, Appl. Catal. A 242 (2003) 41.
[8] A. Louloudi, N. Papayannakos, Appl. Catal. A 175 (1998) 21.
[9] A. Louloudi, N. Papayannakos, Appl. Catal. A 204 (2000) 167.
[10] G. Marcelin, R.F. Vogel, H.E. Swift, J. Catal. 98 (1986) 64.
[11] F. Mittendorfer, J. Hafner, J. Phys. Chem. B 106 (2002) 13299.
[12] R. Molina, G. Poncelet, J. Catal. 199 (2001) 162.
[13] S. Toppinen, T.K. Rantakyla, T. Salmi, J. Aittamaa, Ind. Eng. Chem. Res. 35 (1996) 1824.
[14] R. Badilla-Ohlbaum, H.J. Neuburg, W.F. Graydon, M.J. Phillips, J. Catal. 47 (1977) 273.
[15] M.I. Phillips, P.H. Emmett, J. Catal. 101 (1986) 268.
[16] K.J. Yoon, M.A. Vannice, J. Catal. 82 (1983) 457.
[17] J.M. Basset, G. Dalmai-Imelik, M. Primet, R. Mutin, J. Catal. 37 (1975) 22.
[18] S.D. Lin, M.A. Vannice, J. Catal. 143 (1993) 539.
[19] P. Chou, M.A. Vannice, J. Catal. 107 (1987) 129.
[20] P. Chou, M.A. Vanice, J. Catal. 107 (1987) 140.
[21] C. Milone, G. Neri, A. Donato, M.G. Musolino, J. Catal. 159 (1996) 253.
[22] L. Ronchin, L. Toniolo, Catal. Today 66 (2001) 363.
[23] J.Q. Wang, P.J. Guo, S.R. Yan, M.H. Qiao, H.X. Li, K.N. Fan, J. Mol. Catal. A Chem. 222 (2004) 229.
[24] S.-W. Ho, J.M. Cruz, M. Houalla, D.M. Hercules, J. Catal. 135 (1992) 173.
[25] J.M. Jablonski, D. Potocznapetru, J. Okal, L. Krajczyk, React. Kinet. Catal. Lett. 54 (1995) 15.
[26] W.F. Taylor, J. Catal. 9 (1967) 99.
[27] W.F. Taylor, H.K. Staffin, J. Phys. Chem. 71 (1967) 3314.
[28] L.J. Simon, P.J. Kooyman, J.G. van Ommen, J.A. Lercher, Appl. Catal. A 252 (2003) 283.
[29] P. Tétényi, V. Galsan, Appl. Catal. A 229 (2002) 181.
[30] B. Jongsomjit, J. Panpranot, J.G. Goodwin, J. Catal. 215 (2003) 66.
[31] G. Jacobs, T.K. Das, P.M. Patterson, L. Sanchez, B.H. Davis, Appl. Catal. A 247 (2003) 335.
[32] T.K. Das, G. Jacobs, P.M. Patterson, W.A. Conner, J.L. Li, B.H. Davis, Fuel 82 (2003) 805.
[33] G. Jacobs, P.M. Patterson, Y.Q. Zhang, T. Das, J.L. Li, B.H. Davis, Appl. Catal. A 233 (2002) 215.
[34] G. Jacobs, T.K. Das, Y.Q. Zhang, J.L. Li, G. Racoillet, B.H. Davis, Appl. Catal. A 233 (2002) 263.
[35] G. Jacobs, J.A. Chaney, P.M. Patterson, T.K. Das, J.C. Maillot, B.H. Davis, J. Synchrotron Radiat. 11 (2004) 414.
[36] G. Jacobs, J.A. Chaney, P.M. Patterson, T.K. Das, B.H. Davis, Appl. Catal. A: Gen. 264 (2004) 203.
[37] G. Jacobs, Y.Y. Ji, B.H. Davis, D. Cronauer, A.J. Kropf, C.L. Marshall, Appl. Catal. A 333 (2007) 177.
[38] L. Guczi, D. Bazin, I. Kovacs, L. Borko, Z. Schay, J. Lynch, P. Parent, C. Lafon, G. Stefler, Z. Koppany, I. Sajo, Top. Catal. 20 (2002) 129.
[39] S. Lu, W.W. Lonergan, J.P. Bosco, S. Wang, Y. Zhu, Y. Xie, J.G. Chen, J. Catal. 259 (2008) 260.
[40] S. Lu, C.A. Menning, Y. Zhu, J.G. Chen, Chem. Phys. Chem 10 (2009) 1763.
[41] J.H. Sinfelt, Accounts Chem. Res. 10 (1977) 15.
[42] J.H. Sinfelt, Bimetallic Catalysts: Discoveries, Concepts, and Applications, John Wiley & Sons, New York, 1983.
[43] J.A. Rodriguez, Surf. Sci. Rep. 24 (1996) 225.
[44] B. Hammer, J.K. Nørskov, Surf. Sci. 343 (1995) 211.
[45] D.W. Goodman, J. Phys. Chem. 100 (1996) 13090.
[46] V. Pallassana, M. Neurock, J. Catal. 191 (2000) 301.
[47] J.G. Chen, C.A. Menning, M.B. Zellner, Surf. Sci. Rep. 63 (2008) 201.
[48] J. Greeley, M. Mavrikakis, Nat. Mater. 3 (2004) 810.
[49] H.H. Hwu, J. Eng Jr., J.G. Chen, J. Am. Chem. Soc. 124 (2002) 702.
[50] N.A. Khan, L.E. Murillo, J.G. Chen, J. Phys. Chem. B 108 (2004) 15748.
[51] J.R. Kitchin, J.K. Nørskov, M.A. Barteau, J.G. Chen, Phys. Rev. Lett. 93 (2004) 156801.
[52] C.A. Menning, H.H. Hwu, J.G. Chen, J. Phys. Chem. B 110 (2006) 110, 15471.
[53] L.E. Murillo, A.M. Goda, J.G. Chen, J. Am. Chem. Soc. 129 (2007) 7101.
[54] M.P. Humbert, J.G. Chen, J. Catal 257 (2008) 297.
[55] L. Lin, W. Lin, Y.X. Zhu, B.Y. Zhao, Y.C. Xie, Y. He, Y.F. Zhu, J. Mol. Catal. A: Chem. 236 (2005) 236.
[56] Y. Shu, L.E. Murillo, J.P. Bosco, W. Huang, A.I. Frenkel, J.G. Chen, Appl. Catal. A 339 (2008) 169.
[57] M. Newville, J. Synchrotron Radiat. 8 (2001) 96–100.
[58] B. Ravel, M. Newville, J. Synchrotron Radiat. 12 (2005) 537–541.
[59] J.J. Rehr, R.C. Albers, Rev. Mod. Phys. 72 (2000) 621–654.
[60] H.P. Klug, L.E. Alexander, X-ray Diffraction Procedures for Polycrystalline and Amorphous Materials, John-Wiley, 1974.
[61] E.V. Steen, G.S. Sewell, R.A. Makhothe, C. Mickelethwaite, H. Manstein, M. de Lange, C.T. O'Connor, J. Catal. 162 (1996) 220.
[62] R. Radhakrishnan, S.T. Oyama, J.G. Chen, K. Asakura, J. Phys. Chem. B 105 (2001) 4245.